Fully Arbitrary Control of Frequency-Bin Qubits

Hsuan-Hao Lu,[1,*] Emma M. Simmerman,[2] Pavel Lougovski,[2,†] Andrew M. Weiner,[1] and Joseph M. Lukens[2,‡]
[1]School of Electrical and Computer Engineering and Purdue Quantum Science and Engineering Institute, Purdue University, West Lafayette, Indiana 47907, USA
[2]Quantum Information Science Group, Computational Sciences and Engineering Division, Oak Ridge National Laboratory, Oak Ridge, Tennessee 37831, USA

(Received 18 June 2020; accepted 14 August 2020; published 14 September 2020)

Accurate control of two-level systems is a longstanding problem in quantum mechanics. One such quantum system is the frequency-bin qubit: a single photon existing in superposition of two discrete frequency modes. In this Letter, we demonstrate fully arbitrary control of frequency-bin qubits in a quantum frequency processor for the first time. We numerically establish optimal settings for multiple configurations of electro-optic phase modulators and pulse shapers, experimentally confirming near-unity mode-transformation fidelity for all fundamental rotations. Performance at the single-photon level is validated through the rotation of a single frequency-bin qubit to 41 points spread over the entire Bloch sphere, as well as tracking of the state path followed by the output of a tunable frequency beam splitter, with Bayesian tomography confirming state fidelities $\mathcal{F}_\rho > 0.98$ for all cases. Such high-fidelity transformations expand the practical potential of frequency encoding in quantum communications, offering exceptional precision and low noise in general qubit manipulation.

DOI: 10.1103/PhysRevLett.125.120503

Introduction.—The precise, coherent manipulation of the spectrotemporal properties of light has facilitated a plethora of applications, ranging from radio-frequency arbitrary waveform generation and optical communications [1,2], to coherent control of chemical reactions [3,4] and extreme nonlinear optics [5,6]. Throughout these developments, Fourier-transform pulse shaping has played a central role, enabling arbitrary spectral filters that can shape optical fields on femtosecond timescales [7,8]. Concurrently, the Fourier dual process of electro-optic modulation has been a staple in fiber optics, functioning as "temporal filters" that multiply an input field in the time domain with phase patterns for applications such as optical communication [9] or frequency comb generation [2,10]. The value of complex time-frequency control extends beyond classical optics to photonic quantum information processing (QIP) as well, with demonstrations of temporal shaping [11], spectral coding [12], wave packet modulation [13,14], spread spectrum [15], electro-optic time lensing [16], and high-dimensional quantum state reconstruction [17–19] on single photons and entangled photon pairs.

These successes have inspired the development of a complete QIP paradigm based on pulse shapers, modulators, and frequency-bin encoding [20]. Drawing on arguments from linear-optical quantum computation (LOQC) [21], the "quantum frequency processor" (QFP) approach has been shown scalable in principle, and a collection of gates comprising a universal set have been realized experimentally [22–25]. Such scaling arguments prove crucial in establishing ultimate feasibility, yet leave many smaller—though highly practical—questions unanswered. For example, the fully arbitrary rotation of a single qubit represents a fundamental capability for any two-level system, enjoying a long history as a textbook example in quantum mechanics [26,27]. Yet neither a Solovay-Kitaev construction [28] in terms of basic gates, nor general resource bounds, reveals the optimal construction of general two-mode unitaries, particularly when subject to practical resource constraints.

In this Letter, we answer this important question through theoretical analysis and experimental verification of arbitrary single-qubit gates in frequency-bin encoding. Our numerical simulations obtain three-element QFP configurations capable of any unitary operation with fidelity $\mathcal{F}_W \geq 0.9999$ utilizing single-tone modulation only; by either adding a second harmonic or cascading an additional pulse shaper and modulator pair, such operations achieve success probabilities $\mathcal{P}_W > 0.95$ or $\mathcal{P}_W > 0.999$, respectively. We reinforce these findings experimentally, synthesizing frequency-bin unitaries with performance in close agreement with theory. Finally, we highlight their use at the single-photon level in the rotation of a fixed input to arbitrary points on the Bloch sphere, obtaining output state fidelities $\mathcal{F}_\rho > 0.98$ with respect to the ideal. Our results represent the first full tomography of arbitrarily rotated frequency-bin qubit states, establishing resource guidelines for future systems and providing tools for fundamental applications in communications and coherent control.

Problem formulation.—A frequency-bin qubit can be represented as a single photon in a superposition of two

frequency modes, or bins, described by annihilation (creation) operators $\hat{a}_0$ ($\hat{a}_0^\dagger$) and $\hat{a}_1$ ($\hat{a}_1^\dagger$) centered at frequency ω_0 and ω_1, respectively. A pure qubit state may be expressed as $|\psi\rangle = (c_0\hat{a}_0^\dagger + c_1\hat{a}_1^\dagger)|\text{vac}\rangle$, where $|\text{vac}\rangle$ is the vacuum state and $|c_0|^2 + |c_1|^2 = 1$. Logical basis states follow as $|n\rangle = \hat{a}_n^\dagger|\text{vac}\rangle$ ($n \in \{0, 1\}$). Any 2×2 unitary operating on these modes can be parametrized as [29]

$$U(\theta, \varphi, \lambda) = \begin{pmatrix} \cos\frac{\theta}{2} & -e^{i\lambda}\sin\frac{\theta}{2} \\ e^{i\varphi}\sin\frac{\theta}{2} & e^{i(\varphi+\lambda)}\cos\frac{\theta}{2} \end{pmatrix}, \tag{1}$$

where $\theta \in [0, \pi]$, $\varphi \in [0, 2\pi)$, and $\lambda \in [0, 2\pi)$. Considering this as taking the inputs $\hat{a}_0$ and $\hat{a}_1$ to outputs $\hat{b}_0$ and $\hat{b}_1$, this implies that the output state coefficients, $|\phi\rangle = (d_0\hat{b}_0^\dagger + d_1\hat{b}_1^\dagger)|\text{vac}\rangle$, satisfy $\binom{d_0}{d_1} = U\binom{c_0}{c_1}$.

This mathematical formulation applies generally to any qubit system. The nuances of the QFP approach appear, though, when describing (i) the bins ω_0 and ω_1 as embedded within a comb spaced at $\Delta\omega$ ($\omega_n = \omega_0 + n\Delta\omega; n \in \mathbb{Z}$) and (ii) the transformation on all modes $\hat{b}_m = \sum_n V_{mn}\hat{a}_n$ as characterized by an alternating series of electro-optic phase modulators (EOMs) driven with $(2\pi/\Delta\omega)$-periodic waveforms and pulse shapers applying arbitrary phases to each bin. As modeled, V is unitary over the entire countably infinite collection of bins, though the 2×2 submatrix in the computational space—call this $W = \binom{V_{00}\ V_{01}}{V_{10}\ V_{11}}$—may or may not prove unitary, due to coupling into adjacent bins. While an apparent disadvantage of the QFP in this case (particularly when compared to the isolated modes of alternative frequency-bin approaches [30–35]), this natural coupling between many bins facilitates multiphoton interference between all underlying modes as required for LOQC. Moreover, by cascading additional pulse shapers and EOMs and employing more complex modulation patterns, such adjacent-bin coupling can be fully compensated for, to realize smaller-dimensional gates with unity efficiency [20,36].

Within this overall framework, considerable progress has been made on a subset of $U(\theta, \varphi, \lambda)$: the phase-only gate $U(0, \varphi, \lambda)$ and the Hadamard $H = U(\pi/2, 0, \pi)$, with the former requiring only a single pulse shaper, and the latter realizable with an EOM-pulse shaper-EOM QFP [22,23]. These considerations engender optimism for experimental realization of arbitrary U, yet they do not answer the practical questions of explicit construction, nor elucidate the procedures involved in reconfiguring a given QFP for all possible unitaries.

Numerical simulations.—For our simulations, we focus on pure-sinewave electro-optic modulation (either one or two tones), and QFPs with three or five elements. Limitation to odd-numbered QFPs follows from previous observations that adding a pulse shaper on either side of a QFP improves neither fidelity nor success probability, for any target operation. In fact, these remarks can be made rigorous in the present case of a single-qubit operation. Suppose that a particular QFP configuration realizes the gate $W = gU(\theta, 0, 0)$ (unitary up to an overall constant). Then, as derived in Sec. I. of Ref. [37], the same QFP can actualize the gate $gU(\theta, \varphi, \lambda)$ by delaying the rf signals applied to the first and last EOM and adding linear phases to the first and last pulse shaper (or the single pulse shaper in a three-element QFP).

This finding implies that, for the purpose of establishing performance under system constraints, one need only concentrate on $U(\theta, 0, 0)$ numerically. We emphasize that, while similar, these phase degeneracies prove fundamentally more significant than those resulting from the freedom to set a phase reference. As argued in Ref. [39] and invoked below in our own characterization procedure, the prerogative to define the "in-phase" condition across modes at the input and output planes of an optical multiport simplifies the process of extracting V_{mn}. However, such phase reference flexibility does not imply the physical equivalence of operations that differ by this reference. For example, if one defines the reference so that the QFP realizes $U(\theta, 0, 0)$, modifying the transformation to $U(\theta, \varphi, \lambda)$ produces measurable differences in the output state, impacting any subsequent operations downstream. Accordingly, the relationship between phase and EOM delay discussed here is not just the establishment of a reference: it gives a means to realize a (φ, λ) combination for *any* reference definition.

To benchmark the performance of single-qubit gates synthesized on the QFP, we randomly generate 150 samples of $\theta \in [0, \pi]$, and numerically find the solutions $U(\theta, 0, 0)$ for three different scenarios (see Fig. 1): three-element QFP driven by (i) one or (ii) two rf tones, and (iii) five-element QFP driven by single tone [37]. Case (i) is the baseline QFP which we have utilized in previous experiments [22–24], while cases (ii) and (iii) describe the two most immediate upgrades; (ii) has been explored in a limited context for a frequency-bin qutrit operation [22], while (iii) has so far required too many resources for implementation. Yet all three are realizable with standard, commercially available components. We then assess the performance of W with respect to the desired U according to gate success $\mathcal{P}_W = \text{Tr}(W^\dagger W)/2$ and fidelity $\mathcal{F}_W = |\text{Tr}(W^\dagger U)|^2/(4\mathcal{P}_W)$ metrics, where $\mathcal{P}_W$ describes the probability of a photon remaining in the computational space, and $\mathcal{F}_W$ defines the quality of the operation [40]. Our goal is to maximize $\mathcal{P}_W$ while constraining $\mathcal{F}_W \geq 0.9999$ [37].

Figure 1 plots the simulation results. $\mathcal{P}_W$ shows a strong dependence on θ, suggesting that those unitaries with small θ are easier to realize. This matches our intuition as the identity and phase-only gates ($\theta = 0$) can be realized without any EOM, while gates like Pauli X and Y ($\theta = \pi$) require proper engineering of the mixing process such that

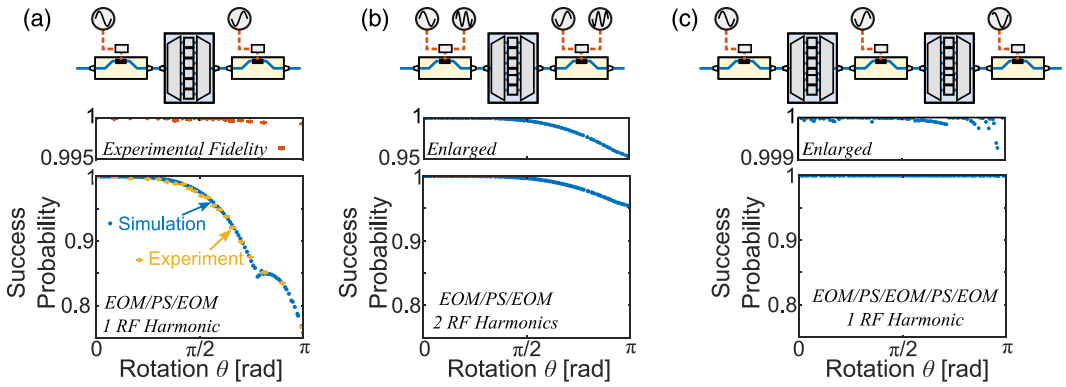

FIG. 1. Optimized success probability of single-qubit gate $U(\theta, 0, 0)$ for different QFP configurations. (a) Three-element QFP, single-tone modulation (including experimental results). (b) Three-element QFP, two-tone modulation. (c) Five-element QFP, single-tone modulation. Enlarged plots for (b) and (c) detail the high-probability regions for each case.

the photon can be completely hopped to the opposite bin. Additionally, the results indicate that gate performance can be significantly boosted by introducing either an additional rf harmonic [Fig. 1(b), $\mathcal{P}_W > 0.95$] or extra components [Fig. 1(c), $\mathcal{P}_W > 0.999$]. Here, we experimentally focus on the setup in Fig. 1(a) due to equipment availability—i.e., insufficient rf amplifier bandwidth for (ii), lack of EOMs, and pulse shapers for (iii).

Gate characterization.—Figure 2 provides a schematic of the experimental setup. A high-frequency rf oscillator generates 25-GHz sinusoidal voltages to drive both EOMs [41], where their amplitudes and delays are set with manual phase shifters and attenuators. Meanwhile, the optimized spectral phase pattern is programmed onto the QFP shaper. Experimentally, we select 21 out of the 150 previous solutions from Fig. 1(a). To investigate whether each gate performs as anticipated, we utilize a coherent-state-based characterization approach [22,39] by probing our QFP with an electro-optic frequency comb. As a result, we are able to

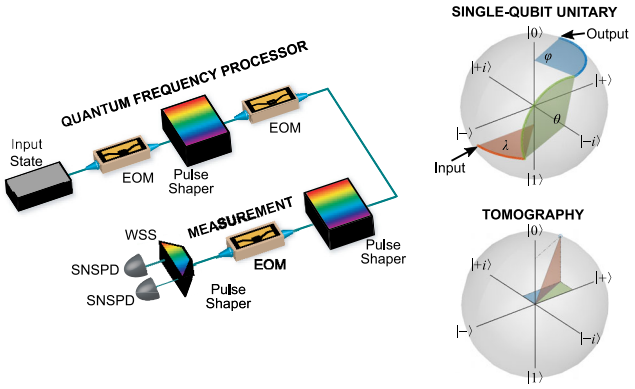

FIG. 2. Experimental setup for arbitrary frequency-qubit operations and state measurement. Insets show an example unitary rotation for an input state $|\psi\rangle = 0.6|0\rangle - 0.8|1\rangle$ and $(\theta, \varphi, \lambda) = (0.7\pi, 0.55\pi, 0.25\pi)$, with tomography represented in terms of projections onto each axis. Here $|\pm\rangle \propto |0\rangle \pm |1\rangle$ and $|\pm i\rangle \propto |0\rangle \pm i|1\rangle$.

reconstruct the mode-transformation matrix W and compute the experimental $\mathcal{F}_W$ and $\mathcal{P}_W$, as shown in Fig. 1(a). All measured gate fidelities are above 0.9993 (except for one, unexplained outlier), and the success probabilities track closely the theoretical prediction.

Arbitrary state rotation.—The previous tests confirm synthesis of arbitrary frequency-qubit operations, when viewed in terms of optical modes. Yet in the context of photonic QIP, these *mode* transformations are valuable insofar as they enable high-fidelity operations on quantum *states*. Accordingly, we explore these gates at the single-photon level, focusing specifically on their ability to convert a fixed input to an arbitrary output state. We can then assess the quality of this manipulation by performing quantum state tomography (QST) on the output photon.

Following the QFP with a set of projective measurements, we reconstruct its density matrix ($\hat{\rho}$) through QST and compute the state fidelity with respect to the ideal output state $|\phi\rangle$ via $\mathcal{F}_\rho = \langle\phi|\hat{\rho}|\phi\rangle$. (Note the change in definition from the Hilbert-Schmidt fidelity $\mathcal{F}_W$ utilized for matrix characterization.) We prepare a single-photon-level source by attenuating a continuous-wave laser at frequency ω_0 to $\sim 10^6$ counts/s (1/10 of the detector saturation level) prior to the QFP. Since neither the QFP operation nor QST involve multiphoton interference, the results of a weak coherent state are fully equivalent to those of true single photons at the same average flux. To show that we can bring this input state, $|0\rangle = \hat{a}_0^\dagger|\text{vac}\rangle$, at the north pole of the Bloch sphere, to any arbitrary state within the whole sphere, we choose 11 values of $\theta \in [0, \pi]$ and assign a few different φ to each, amounting to a total of 41 gates to implement. The ideal output state is $|\phi\rangle = \cos(\theta/2)|0\rangle + e^{i\varphi}\sin(\theta/2)|1\rangle$.

For single-qubit QST [37], we perform three Pauli measurements (Z, X, and Y) to project the output state onto the eigenvectors $|t\rangle$ (six in total): $\{|0\rangle, |1\rangle, |\pm\rangle, |\pm i\rangle\}$. Measuring in Z, X, and Y is equivalent to applying $\mathbb{1}$, H, and $HS^\dagger$ prior to computational-basis projection,

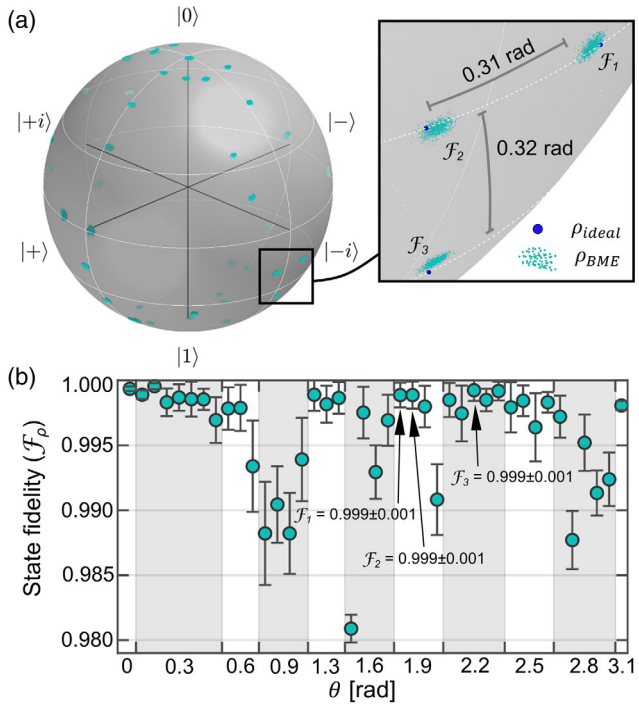

FIG. 3. Arbitrary single-qubit rotations on the QFP. (a) Retrieved Bayesian samples plotted on the Bloch sphere (green dots) following 41 different transformations $U(\theta, \varphi, 0)$. Three examples are highlighted in the inset, where blue dots mark the corresponding ideal states. (b) Associated state fidelities, grouped by θ value, with each data point corresponding to a randomly chosen φ. The mean and standard deviation are computed from 1024 Bayesian samples.

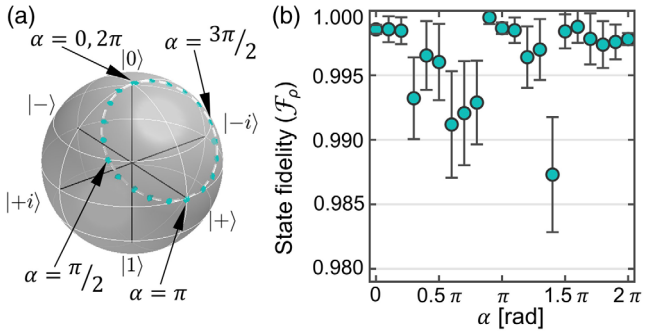

FIG. 4. Tunable beam splitter. (a) Ideal output state trajectory (dashed line) and retrieved Bayesian samples (green dots) plotted on the Bloch sphere. (b) Bayesian state fidelities as function of pulse shaper phase α.

where $S = \left(\begin{smallmatrix} 1 & 0 \\ 0 & i \end{smallmatrix}\right)$. Z measurement demultiplexes the photons by color with a wavelength-selective switch (WSS), and records the counts in $|0\rangle$ and $|1\rangle$ with superconducting nanowire detectors. For the H required for tomography, we implement a simpler probabilistic Hadamard gate based on a single EOM, with a sinusoidal rf voltage chosen for equal mixing probability between ω_0 and ω_1 [37,42]. We precede this EOM with another pulse shaper to apply the $S^\dagger$ gate and block any residual photons outside of the single-qubit space after the QFP. For each measurement setting, we record the counts over 1 s, then subtract the average detector dark counts and obtain a final dataset $\mathcal{D} = \{N_0, N_1, N_+, N_-, N_{+i}, N_{-i}\}$ with all outcomes for subsequent tomographic analyses.

For reconstruction, we employ Bayesian mean estimation [43], an advanced tomographic technique which avoids unjustifiably low-rank estimates and furnishes natural error bars. We parametrize the density matrix $\hat{\rho}(\mathbf{x})$ and sample a posterior distribution $\pi(\mathbf{x}) \propto L_{\mathcal{D}}(\mathbf{x})\pi_0(\mathbf{x})$ with multinomial likelihood $L_{\mathcal{D}}(\mathbf{x}) = p_0^{N_0} p_1^{N_1} p_+^{N_+} p_-^{N_-} p_{+i}^{N_{+i}} p_{-i}^{N_{-i}}$, where $p_t \equiv \langle t|\hat{\rho}(\mathbf{x})|t\rangle$ is the probability of measuring the state $|t\rangle$ given the proposed state $\hat{\rho}(\mathbf{x})$. We adopt the parametrization, prior distribution $\pi_0(\mathbf{x})$, and sampling procedure recently proposed in Ref. [44], obtaining $R = 1024$ density matrix samples $\hat{\rho}_r$ for each tomographic dataset, from which we estimate the fidelity according to the mean and standard deviation of the values of the individual samples ($\mathcal{F}_r = \langle\phi|\hat{\rho}_r|\phi\rangle$).

Figure 3 depicts the QST results. We map the ideal output states and the retrieved Bayesian samples onto the Bloch sphere [Fig. 3(a)]. Three of the transformations are highlighted in the enlarged inset, where the Bayesian samples follow the ideal states closely. This suggests strong agreement between the design and experimental implementation, confirmed by Bayesian mean state fidelities above 98% across all gates [Fig. 3(b)].

Tunable beam splitter.—In addition to a randomly chosen set of single-qubit rotations, we can also explore coherent quantum state control across a specified trajectory. Previously, we found a set of analytical solutions for tunable frequency beam splitters [23], where the reflectivity can be set anywhere between 0 and 0.5 simply by changing the depth of the phase shift α imparted by the QFP shaper between frequency bins 0 and 1 (while both EOMs remain fixed) [37]. We sample 21 evenly spaced $\alpha \in [0, 2\pi]$ for implementation, and again repeat the QST measurement for the same state input $|0\rangle$. Figure 4 depicts the experimental results. As we increase α, the output state is moved from the north pole ($|0\rangle$) to the equator ($|+\rangle = H|0\rangle$), and then back to the north pole ($|0\rangle$), following a counterclockwise trajectory on the Bloch sphere (dashed line in Fig. 4) [37]. Again all measurements are in excellent agreement with theory ($\mathcal{F}_\rho > 0.98$).

Discussion.—In addition to addressing fundamental questions in frequency-bin quantum state control, the findings described here appear particularly relevant in the applications of quantum communications and networking. Indeed, one of the inherent benefits of frequency-bin encoding is its compatibility with fiber-optic communications: the QFP paradigm already leverages commercial telecom components (EOMs and pulse shapers), and frequency-bin operations can be extensively parallelized according to the principles of wavelength-division multiplexing (WDM). This synergy has enabled several

recent quantum networking demonstrations invoking WDM for distributing entanglement in other degrees of freedom [45–48]; the QFP approach moves even further by exploiting frequency bins for encoding quantum information as well, and the fully arbitrary unitaries realized here should make feasible an array of quantum networking protocols with frequency bins. Whereas the previously shown Hadamard ($\theta = \pi/2$) [22,23] would be sufficient (along with the identity) for basis measurements in quantum key distribution [49], it is only through these more general unitaries that the full range of qubit quantum information protocols can be realized. For example, both superdense coding [50] and quantum teleportation [51] require single-qubit gates including a full 180° rotation ($\theta = \pi$), and the standard CHSH Bell inequality [52] relies on measurements preceded by unitaries with $\theta \in [0, \pi/4, \pi/2, 3\pi/4]$.

Moreover, while we have focused specifically on the fundamental two-level qubit here, one of the salient features of the frequency degree of freedom is its natural compatibility with high-dimensional qudit ($d > 2$) encoding [18,19,53,54]. Importantly, the same design procedure adopted here can be applied for the construction of arbitrary qudit operations as well. As initial examples, we have numerically found $2d + 1$ EOMs and pulse shapers sufficient for high-dimensional frequency hopping (up to $d = 5$) using single-tone rf modulation [36]; we have also found $d - 1$ rf harmonics capable of realizing d-dimensional discrete Fourier transformations (up to $d = 10$) on a single three-element QFP. The main limitations in moving to higher dimensions, then, are technical in nature—namely, the complexity of rf drive waveforms and the number of pulse shapers and EOMs available.

On the characterization side, our focus on QST of an arbitrarily rotated state corroborates the gate performance estimated from classical measurements. On the other hand, quantum process tomography (QPT) would be required for a complete quantum-mechanical description of the gate itself [55]. This procedure relies on preparation of multiple input states (four in the case of a single-qubit operation), followed by QST of each output after the QFP, which would necessitate additional components beyond those available to us. Given our understanding of the physical mechanisms involved in the QFP, we do not expect fundamentally new insights from QPT. Nevertheless, realization of complete QPT—perhaps leveraging Bayesian techniques for experimental simplifications—would prove valuable in future work, as a means to further validate performance.

This research was performed in part at Oak Ridge National Laboratory, managed by UT-Battelle, LLC, for the U.S. Department of Energy under Contract No. DE-AC05-00OR22725. Funding was provided by the U.S. Department of Energy, Office of Science (Office of Advanced Scientific Computing Research, Early Career Research Program; and Office of Workforce Development for Teachers and Scientists Science Undergraduate Laboratory Internship Program) and the National Science Foundation (Grant No. 1839191-ECCS).

*lu548@purdue.edu
†Present affiliation: Amazon Web Services, Seattle, Washington 98109, USA
‡lukensjm@ornl.gov

[1] S. T. Cundiff and A. M. Weiner, Nat. Photonics **4**, 760 (2010).
[2] V. Torres-Company and A. M. Weiner, Laser Photonics Rev. **8**, 368 (2014).
[3] R. Teets, J. Eckstein, and T. Hänsch, Phys. Rev. Lett. **38**, 760 (1977).
[4] Y. Silberberg, Annu. Rev. Phys. Chem. **60**, 277 (2009).
[5] A. Baltuška, T. Udem, M. Uiberacker, M. Hentschel, E. Goulielmakis, C. Gohle, R. Holzwarth, V. Yakovlev, A. Scrinzi, T. W. Hänsch *et al.*, Nature (London) **421**, 611 (2003).
[6] M. T. Hassan, A. Wirth, I. Grguraš, A. Moulet, T. T. Luu, J. Gagnon, V. Pervak, and E. Goulielmakis, Rev. Sci. Instrum. **83**, 111301 (2012).
[7] A. M. Weiner, Rev. Sci. Instrum. **71**, 1929 (2000).
[8] A. M. Weiner, Opt. Commun. **284**, 3669 (2011).
[9] I. Kaminow, T. Li, and A. E. Willner, *Optical Fiber Telecommunications VB: Systems and Networks* (Elsevier, Amsterdam, 2010).
[10] A. J. Metcalf, V. Torres-Company, D. E. Leaird, and A. M. Weiner, IEEE J. Sel. Top. Quantum Electron. **19**, 231 (2013).
[11] A. Pe'er, B. Dayan, A. A. Friesem, and Y. Silberberg, Phys. Rev. Lett. **94**, 073601 (2005).
[12] J. M. Lukens, A. Dezfooliyan, C. Langrock, M. M. Fejer, D. E. Leaird, and A. M. Weiner, Phys. Rev. Lett. **112**, 133602 (2014).
[13] P. Kolchin, C. Belthangady, S. Du, G. Y. Yin, and S. E. Harris, Phys. Rev. Lett. **101**, 103601 (2008).
[14] C. Liu, Y. Sun, L. Zhao, S. Zhang, M. M. T. Loy, and S. Du, Phys. Rev. Lett. **113**, 133601 (2014).
[15] C. Belthangady, C.-S. Chuu, I. A. Yu, G. Y. Yin, J. M. Kahn, and S. E. Harris, Phys. Rev. Lett. **104**, 223601 (2010).
[16] M. Karpiński, M. Jachura, L. J. Wright, and B. J. Smith, Nat. Photonics **11**, 53 (2017).
[17] C. Bernhard, B. Bessire, T. Feurer, and A. Stefanov, Phys. Rev. A **88**, 032322 (2013).
[18] M. Kues, C. Reimer, P. Roztocki, L. R. Cortés, S. Sciara, B. Wetzel, Y. Zhang, A. Cino, S. T. Chu, B. E. Little, D. J. Moss, L. Caspani, J. Azaña, and R. Morandotti, Nature (London) **546**, 622 (2017).
[19] P. Imany, J. A. Jaramillo-Villegas, O. D. Odele, K. Han, D. E. Leaird, J. M. Lukens, P. Lougovski, M. Qi, and A. M. Weiner, Opt. Express **26**, 1825 (2018).
[20] J. M. Lukens and P. Lougovski, Optica **4**, 8 (2017).
[21] E. Knill, R. Laflamme, and G. J. Milburn, Nature (London) **409**, 46 (2001).
[22] H.-H. Lu, J. M. Lukens, N. A. Peters, O. D. Odele, D. E. Leaird, A. M. Weiner, and P. Lougovski, Phys. Rev. Lett. **120**, 030502 (2018).

[23] H.-H. Lu, J. M. Lukens, N. A. Peters, B. P. Williams, A. M. Weiner, and P. Lougovski, Optica **5**, 1455 (2018).

[24] H.-H. Lu, J. M. Lukens, B. P. Williams, P. Imany, N. A. Peters, A. M. Weiner, and P. Lougovski, npj Quantum Inf. **5**, 24 (2019).

[25] H.-H. Lu, A. M. Weiner, P. Lougovski, and J. M. Lukens, IEEE Photonics Technol. Lett. **31**, 1858 (2019).

[26] C. P. Slichter, *Principles of Magnetic Resonance*, 3rd ed. (Springer-Verlag, Berlin, 1990).

[27] L. Mandel and E. Wolf, *Optical Coherence and Quantum Optics* (Cambridge University Press, Cambridge, England, 1995).

[28] C. M. Dawson and M. A. Nielsen, arXiv:quant-ph/0505030.

[29] M. A. Nielsen and I. L. Chuang, *Quantum Computation and Quantum Information* (Cambridge University Press, Cambridge, England, 2000).

[30] M. G. Raymer, S. J. van Enk, C. J. McKinstrie, and H. J. McGuinness, Opt. Commun. **283**, 747 (2010).

[31] H. J. McGuinness, M. G. Raymer, C. J. McKinstrie, and S. Radic, Phys. Rev. Lett. **105**, 093604 (2010).

[32] T. Kobayashi, R. Ikuta, S. Yasui, S. Miki, T. Yamashita, H. Terai, T. Yamamoto, M. Koashi, and N. Imoto, Nat. Photonics **10**, 441 (2016).

[33] S. Clemmen, A. Farsi, S. Ramelow, and A. L. Gaeta Phys. Rev. Lett. **117**, 223601 (2016).

[34] M. Zhang, C. Wang, Y. Hu, A. Shams-Ansari, T. Ren, S. Fan, and M. Lončar, Nat. Photonics **13**, 36 (2019).

[35] C. Joshi, A. Farsi, A. Dutt, B. Y. Kim, X. Ji, Y. Zhao, A. M. Bishop, M. Lipson, and A. L. Gaeta, Phys. Rev. Lett. **124**, 143601 (2020).

[36] J. M. Lukens, H.-H. Lu, B. Qi, P. Lougovski, A. M. Weiner, and B. P. Williams, J. Lightwave Technol. **38**, 1678 (2020).

[37] See the Supplemental Material at http://link.aps.org/supplemental/10.1103/PhysRevLett.125.120503 for derivation of unitary operation symmetries, details on the numerical optimization approach, quantum state measurement settings, and tunable beam splitter design, which includes Refs. [22,23,38].

[38] K. E. Parsopoulos and M. N. Vrahatis, in *Intelligent Technologies–Theory and Application: New Trends in Intelligent Technologies* (IOP Press, 2002), pp. 214–226.

[39] S. Rahimi-Keshari, M. A. Broome, R. Fickler, A. Fedrizzi, T. C. Ralph, and A. G. White, Opt. Express **21**, 13450 (2013).

[40] D. B. Uskov, L. Kaplan, A. M. Smith, S. D. Huver, and J. P. Dowling, Phys. Rev. A **79**, 042326 (2009).

[41] In our experiments, we take $\omega_0/2\pi = 193.575$ THz (1548.25 nm). This number can be chosen anywhere within the passband of the central pulse shaper (1530–1570 nm) without performance degradation. Our frequency-bin spacing ($\Delta\omega/2\pi = 25$ GHz) is chosen between the spectral resolution of the pulse shaper (∼10 GHz) and the bandwidth of the rf components (∼30 GHz). Neither absolute or relative frequency scales impact the theoretical model. See Ref. [22] for details.

[42] P. Imany, O. D. Odele, M. S. Alshaykh, H.-H. Lu, D. E. Leaird, and A. M. Weiner, Opt. Lett. **43**, 2760 (2018).

[43] R. Blume-Kohout, New J. Phys. **12**, 043034 (2010).

[44] J. M. Lukens, K. J. H. Law, A. Jasra, and P. Lougovski, New J. Phys. **22**, 063038 (2020).

[45] H. C. Lim, A. Yoshizawa, H. Tsuchida, and K. Kikuchi, Opt. Express **16**, 16052 (2008).

[46] D. Aktas, B. Fedrici, F. Kaiser, T. Lunghi, L. Labonté, and S. Tanzilli, Laser Photonics Rev. **10**, 451 (2016).

[47] S. Wengerowsky, S. K. Joshi, F. Steinlechner, H. Hübel, and R. Ursin, Nature (London) **564**, 225 (2018).

[48] N. B. Lingaraju, H.-H. Lu, S. Seshadri, D. E. Leaird, A. M. Weiner, and J. M. Lukens, in *Conference on Lasers and Electro-Optics, OSA Technical Digest* (Optical Society of America, 2020) paper FTh1D.2, https://www.osapublishing.org/abstract.cfm?uri=CLEO_QELS-2020-FTh1D.2.

[49] N. Gisin, G. Ribordy, W. Tittel, and H. Zbinden, Rev. Mod. Phys. **74**, 145 (2002).

[50] C. H. Bennett and S. J. Wiesner, Phys. Rev. Lett. **69**, 2881 (1992).

[51] C. H. Bennett, G. Brassard, C. Crépeau, R. Jozsa, A. Peres, and W. K. Wootters, Phys. Rev. Lett. **70**, 1895 (1993).

[52] J. F. Clauser, M. A. Horne, A. Shimony, and R. A. Holt, Phys. Rev. Lett. **23**, 880 (1969).

[53] R. Ikuta, R. Tani, M. Ishizaki, S. Miki, M. Yabuno, H. Terai, N. Imoto, and T. Yamamoto, Phys. Rev. Lett. **123**, 193603 (2019).

[54] M. Erhard, M. Krenn, and A. Zeilinger, Nat. Rev. Phys. **2**, 365 (2020).

[55] I. L. Chuang and M. A. Nielsen, J. Mod. Opt. **44**, 2455 (1997).